Frontiers in Health Informatics
ISSN-Online: 2676-7104
www.healthinformaticsjournal.com
2024; Vol 13: Issue 4
Open Access

Structural, Spectroscopic Investigations And Molecular Docking Analysis Of Benzilic Acid

S. Sundararaj [a,i], M. Amalanathan[b*,i], M. Sony Michael Mary[c,i]

[a]Research Scholar, Reg No: 22113102131001, Nanjil Catholic College of Arts & Science, Kaliyakkavilai-629 153, Affiliated to Manonmaniam Sundaranar University, Abishekapatti, Tirunelveli-627 012, Tamil Nadu, India.

[b*]Department of Physics & Research Centre, Nanjil Catholic College of Arts & Science, Kaliyakkavilai, Affiliated to Manonmaniam Sundaranar University, Abishekapatti, Tirunelveli-627 012, Tamil Nadu, India.

[c]Department of Physics, Annai Velankanni College, Tholayavattam - 629157, Affiliated to Manonmaniam Sundaranar University, Abishekapatti, Tirunelveli-627 012, Tamil Nadu, India.

Corresponding author: Dr.M.Amalanathan, nathan.amalphysics@gmail.com

Cite this paper as: S. Sundararaj, M. Amalanathan, M. Sony Michael Maryc(2024) Structural, Spectroscopic Investigations And Molecular Docking Analysis Of Benzilic Acid. *Frontiers in Health Informatics,* (4), 2183-2211

Abstract

In the present study, a detailed quantum chemical investigation was performed to explore the structural, vibrational, and topological characteristics of the title compound. The molecular geometry was optimized using Density Functional Theory (DFT) at the B3LYP/6-311++G(d,p) level, and the corresponding structural parameters were determined. Natural Bond Orbital (NBO) analysis revealed significant intra- and intermolecular interactions, confirming the compound's bioactive potential. The HOMO–LUMO analysis was done in order to confirm the pharmaceutical nature of molecule. The experimental FT-IR and FT-Raman spectra were recorded and found to be in good agreement with the theoretical vibrational frequencies analyzed using VEDA software. Non-Covalent Interaction (NCI) analysis highlighted the presence of both strong and weak intermolecular forces, while Molecular Electrostatic Potential (MEP), Electron Localization Function (ELF), Localized Orbital Locator (LOL), and Atoms in Molecules (AIM) analyses identified the reactive regions and electron density distribution of the molecule. Drug-likeness evaluation suggested favorable pharmacological properties, supporting the compound's potential as an active therapeutic agent. Molecular docking studies were also carried out.

1. Introduction

Benzilic acids and their derivatives have attracted significant attention in the past decades. Highly pure benzilic acids are used as a pharmaceutical drug [1]. Benzilic acid salts are found to be useful in the treatment of rhinitis [2, 3]. Benzil-benzilic acid rearrangement is a key factor for the preparation of more number of organic compounds. This rearrangement is used to synthesise A-Norpregnanes [4].

The molecular conformations are of particular interest because they are expected to form intermolecular and intramolecular hydrogen bonding in solution and solid state. In addition molecular design of benzilic acid, containing one electron donor and one electron acceptor moiety provides it with a push-pull configuration. Benzilic acid also acts as corrosion inhibiting species with metal oxyanions [5]. Derivatives of benzilic acid are less soluble than hydroxy acids, which exhibit corrosion inhibiting compound with maximum solubility. Certain derivative of benzilic acid acts as suitable corrosion inhibitors for specific metals and their alloys. The benzilic acid acts as a multifunctional ligand, in that it has the potential to coordinate in a number of different ways [6-9]. Using hydrothermal synthetic method, many frameworks are built by benzilate anion with transition metal ions or rare earth ions [9].

The advent of fast computers along with sophisticated computational methods makes the task of solving various structural recently become an efficient tool in the prediction of molecular structure, harmonic force fields, vibrational wavenumbers, IR and Raman activities of Coumarin derivatives compounds [9,10]. The spectroscopic study (IR, Raman) may also be used in the evaluation of the molecular groups present in the compound, electronic charge distribution and aromaticity of molecules. In recent years, the vibrational spectral investigation and NMR spectroscopy play a vital role in the investigations of coumarin derivatives and the identification of the structure activity relationship. However, to the best of our knowledge a complete vibrational analysis of 6-Metyl Coumarin(BA) has not yet been made. Therefore, the present investigation has been undertaken to study the vibrational spectra and NMR analysis of this molecule completely and to identify the various modes with greater wavenumber accuracy by using the DFT computation. The present work reports the results of a systematic study of the geometrical and electronic structure, electrostatic potential surfaces, NMR and vibrational spectra of Benzilic acid (BA) based on their experimental, Infrared and Raman spectra and density functional theory (DFT) computations. The natural bond orbital (NBO) analysis explains the hydrogen bonding and the electronic effects. The charge analysis shows the charge transfer interactions of the molecules.

2. Experimental

The FT-IR spectrum of BA molecule which was recorded in the region 4000–400 cm-1 on Perkin Elmer Spectrum1 spectrophotometer using KBr pellet. The spectral resolution is ±1 cm-1. The FT-Raman spectrum of BA molecule has been recorded with Bruker BRUKER: RFS 27 in the region 50–3500 cm-1 using 1064 nm line of Nd:YAG laser as excitation. The spectra were recorded with spectral resolution of 2 cm-1.

3. Computational

All the calculations were performed using Gaussian 09W program package [11] with the default convergence criteria. The BA was optimized without any constraint and the harmonic wavenumbers were performed to convince the optimized structures in their stable ground states using Density functional Becke3–Lee–Yang–Parr (DFT/B3LYP) level with standard 6-31G(d) and B3LYP6-311++G (d, p) [12] basis set were adopted to calculate the structure and vibrational wavenumbers of

the molecule. The calculated vibrational wavenumbers were assigned with the aid of the Gauss View program [13]. The computed optimized geometry and the corresponding parameters showed the minimum energy conformation. The minimum energy is obtained by solving self consistent field equation iteratively. The harmonic vibrational wavenumbers have been analytically calculated by taking the second- order derivative of energy using the similar level theory. The calculated vibrational wavenumber was scaled down by using the scaling factor 0.9614, 9670 [14] for the B3LYP/6-31G(d) and B3LYP/6-311++G(d,p) level to offset the systematic error caused by neglecting anharmonicity and electron density. The vibrational modes were assigned on the basis of PED analysis using VEDA 4 program [15]. The internal co-ordinates were optimized repeatedly to maximize the PED contributions. The Raman activities (Si) calculated with Gaussian '09 program converted to relative Raman intensities (Ii) using the following relationship derived from the intensity theory of Raman scattering [16,17] given by Eqn. (1) as:

$$I_i = \frac{f(\nu_o - \nu_i)^4 S_i}{\nu_i \left[1 - \exp\left(\frac{-hc\nu_i}{kT}\right)\right]} \qquad (4.1)$$

where ν0 is the exciting wavenumber, ni is the vibrational wavenumber of the ith normal mode, h, c, and k are universal constants, and 'f ' is a suitably chosen common scaling factor for all the peak intensities. The simulated IR and Raman spectra were plotted using pure Lorentzian band shapes with a FWHM of 10 cm-1.

4. Result and Discussion:

4.1 Optimized Geometry

For doing theoretical calculations the initial parameters were taken from and structural optimizations has been done with B3LYP method and 6-311+G(d,p) as basis set. The optimized bondlengths, bond angles and diheadral angles for BA are compared with XRD[18]. From the Table 1 one can find that most of the optimized bond lengths, bond angles are larger than experimental values, due to the fact that the theoretical calculations belongs to isolated molecule in gaseous phase and experimental results belongs to molecule in solid stat. The most stable optimized geometry obtained from B3LYP6-311++G (d, p) method and the scheme of numbering of atoms of the molecules BA is shown in Figure 1. Molecular symmetry can be used to predict many molecular properties such as its dipole moment and its allowed spectroscopic transitions. The most optimized structural parameters (bond length and bond angle) calculated by B3LYP with 6-31G(d,p) and 6-311++G (d, p) basis set are presented in Table 1. From the table the most of the bond lengths and bond angles parameters of ring molecules are in the normal ranges. The C26-O27 (1.2118 Å) bond length is decreased from the normal bond length of C-O due to the possibility of hydrogen bonding present in the molecule between O27……H18. The C12-O24 bond length is elongated than the normal value due to the single bond C-O character nature. The C12–C13(1.5433Å), C3–C12(1.341Å),and C12–C26 (1.5413 Å) bond lengths are longer than the other C–C bonds, which shows the conjugation of electron donor oxygen to the acceptor carbon atom of the ring. This is evident from the atoms angles C3–C12–C13 and C3–C12–O26, whose bond angles

are 113.5º and 111.5º and they are lowering from the other angles in the ring[19].

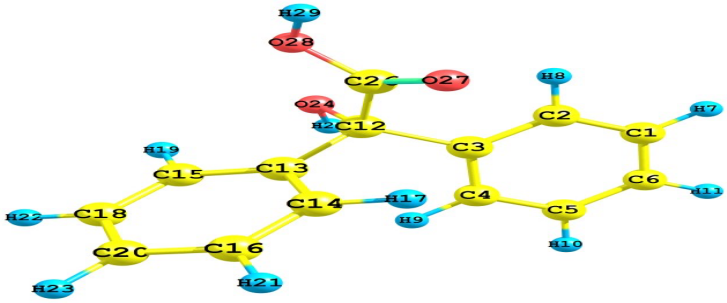

Figure 1: Optimized structure of Benzilic acid calculated at DFT Level

Table 1: Optimized geometric parameters of BA at DFT calculations.

Bond Length	Value (Å)		Bond Angle	Value (Å)		Diheadral Angle	Value (Å)	
	B3LYP/6-31(d) Cal.	B3LYP 6-311++G (d, p)		B3LYP/6-31(d)	B3LYP6-311++G (d, p)		B3LYP/6-31(d) Cal.	B3LYP 6-311++G (d, p)
C_1-C_2	1.393	1.3928	C_1-C_2-C_3	120.6	120.6	C_1-C_2-C_3-C_4	-0.87	-0.84
C_2-C_3	1.4028	1.4025	C_2-C_3-C_4	118.5	118.6	C_2-C_3-C_4-C_5	0.62	0.58
C_3-C_4	1.4009	1.4008	C_3-C_4-C_5	120.7	120.7	C_3-C_4-C5-C6	-0.04	-0.03
C_4-C_5	1.3969	1.3966	C_4-C_5-C_6	120.1	120.1	C_3-C_2-C_1-H_7	-179.38	-179.38
C_5-C_6	1.3938	1.3936	C_2-C_1-H_7	119.5	119.5	C_6-C_1-C_2-H_8	179.90	179.78
C_1-H_7	1.0867	1.086	C_1-C_2-H_8	119.3	119.4	C_2-C_3-C_4-H_9	179.97	179.92
C_2-H_8	1.0849	1.0843	C_3-C_4-H_9	119.7	119.7	C_3-C_4-C_5-H_{10}	-179.39	179.68
C_4-H_9	1.0854	1.0849	C_4-C_5-H_10	119.5	119.5	C_4-C_5-C_6-H_{11}	179.60	179.59
C_5-H_{10}	1.0868	1.0861	C_5-C_6-H_{11}	120.2	120.2	C_1-C_2-C_3-C_{12}	-173.27	-173.26
C_6-H_{11}	1.0867	1.0861	C_2-C_3-C_{12}	120.5	120.6	C_2-C_3-C_{12}-C_{13}	-156.67	-156.12
C_3-C_{12}	1.5341	1.5342	C_3-C_{12}-C_{13}	113.5	113.4	C_3-C_{12}-C_{13}-C_{14}	54.44	54.65
C_{12}-C_{13}	1.5433	1.5432	C_{12}-C_{13}-C_{14}	120.4	120.4	C_3-C_{12}-C_{13}-C_{15}	-127.82	-127.54
C_{13}-C_{14}	1.4026	1.4024	C_{12}-C_{13}-C_{15}	120.2	120.2	C_{12}-C_{13}-C_{14}-C_{16}	178.88	178.92
C_{13}-C_{15}	1.3974	1.3972	C_{13}-C_{14}-C_{16}	120.2	120.2	C_{12}-C_{13}-C_{14}-H_{17}	-0.66	-0.59
C_{14}-C_{16}	1.3938	1.3935	C_{13}-C_{14}-H_{17}	119.5	119.5	C_{12}-C_{13}-C_{15}-C_{18}	-179.09	-179.13
C_{14}-H_{17}	1.0858	1.0853	C_{13}-C_{15}-C_{18}	120.3	120.2	C_{12}-C_{13}-C_{15}-H_{19}	0.16	0.154
C_{15}-C_{18}	1.397	1.3968	C_{13}-C_{15}-H_{19}	119.0	119.0	C_{13}-C_{15}-C_{18}-C_{20}	-0.24	0.64
C_{15}-H_{19}	1.0844	1.0839	C_{15}-C_{18}-C_{20}	120.2	120.2	C_{13}-C_{14}-C_{16}-H_{21}	179.86	179.87
C_{18}-C_{20}	1.3946	1.3943	C_{14}-C_{16}-H_{21}	119.6	119.6	C_{13}-C_{15}-C_{18}-H_{22}	-179.74	-179.74

C_{16}-H_{21}	1.0868	1.0862	C_{15}-C_{18}-H_{22}	119.5	119.6	C_{15}-C_{18}-C_{20}-H_{23}	179.88	179.89
C_{18}-H_{22}	1.0869	1.0863	C_{18}-C_{20}-H_{23}	120.2	120.2	C_2-C_3-C_{12}-O_{24}	78.73	79.32
C_{20}-H_{23}	1.0868	1.0861	C_3-C_{12}-O_{24}	108.4	108.5	C_3-C_{12}-O_{24}-H_{25}	43.77	42.90
C_{12}-O_{24}	1.4307	1.4296	C_{12}-O_{24}-H_{25}	106.3	106.8	C_2-C_3-C_{12}-C_{26}	-38.63	-38.17
O_{24}-H_{25}	0.9709	0.9672	C_3-C_{12}-C_{26}	111.5	111.6	C_3-C_{12}-C_{26}-O_{27}	-38.20	-37.90
C_{12}-C_{26}	1.5413	1.5418	C_{12}-C_{26}-O_{27}	124.1	124.1	C_3-C_{12}-C_{26}-O_{28}	145.60	145.90
C_{26}-O_{27}	1.2118	1.212	C_{12}-C_{26}-O_{28}	112.6	112.6	C_{12}-C_{26}-O_{28}-H_{29}	175.39	175.41
C_{26}-O_{28}	1.3461	1.345	C_{26}-O_{28}-H_{29}	105.4	105.5			
O_{28}-H_{29}	0.9763	0.9726						

4.2 NBO analysis

In order to obtain a more complete picture of the electronic structure of the molecules in the BA molecule, the main natural orbital interactions were analyzed with the NBO 5.0 program [20] both for the single point structure and its optimized counterpart. The lowering of orbital energy due to the interaction between doubly occupied orbitals and unoccupied ones are very convenient guide to interpret the molecular structure in the electronic point of view. In energetic terms, hyperconjugation is an important effect [21,22] in which an occupied Lewis-type natural bond orbital is stabilized by overlapping with a non-Lewis-type orbital (either one-center Rydberg or two-center antibonding NBO). This electron delocalization can be described as a charge transfer from a Lewis valence orbital (donor) with a decreasing of its occupancy, to a non-Lewis orbital (acceptor). Several other types of valuable data such as directionality, hybridization and partial charges were analyzed in the output of NBO analysis. The NBO [19-22] analysis is already proved to be an effective tool for chemical interpretation of hyperconjugative interaction and electron density transfer from the filled lone pair electron. The hyper-conjugative interaction energy was deduced from the second-order perturbation approach.

$$E(2) = -n_\sigma \frac{\langle \sigma | F | \sigma \rangle^2}{\varepsilon_{\sigma^*} - \varepsilon_\sigma} = -n_\sigma \frac{F_{ij}^2}{\Delta E} \qquad (2)$$

where $\langle \sigma | F | \sigma \rangle^2$, or F^2_{ij} is the Fock matrix element between i and j NBO orbitals, ε_σ and ε_{σ^*} are the energies of σ and σ* NBO's, and n_σ is the population of the donor σ orbital. NBO theory can also be used to identify hydrogen bonding.

Table 2 shows the most important interactions between Lewis and non-Lewis orbitals with O lone pairs, the second order perturbation energy values, E(2), corresponding to these interactions, and the overlap integral of each orbital pair. A very strong interaction has been observed between the π-type orbital containing the lone electron pair of O1 and the neighbor π*(C5–C6), π*(C1–O7) antibonding orbital of the ring with high stabilization energy 54.60 and 47.99 kJ mol−1 respectively. The π electrons of C5 movement towards the n(LP2 O1) orbital and the overlap of the donor and acceptor orbitals are

important interaction for the responsibility of the activity of the molecule. This interaction is responsible for a pronounced decrease of the lone pair orbital occupancy 1.73482 than the other occupancy, and there is a possibility for hyperconjugation between O1 and the benzene ring.

Table 2: Second order perturbation theory analysis of Fock matrix in NBO basis.

Donar	Occupancy (e)	Acceptor	Occupancy (e)	E(2) kcal/mol	E(j)-E(j) a.u.	F(i,j) a.u.
π(C1-C2)	1.6684	π*(C3-C4)	0.3478	19.98	0.29	0.068
		π*(C5-C6)	0.3181	20.64	0.29	0.069
π(C3-C4)	1.6733	π*(C1-C2)	0.3044	19.67	0.29	0.068
		π*(C5-C6)	0.3181	19.50	0.29	0.067
π(C5-C6)	1.6708	π*(C3-C4)	0.3478	19.50	0.29	0.068
		π*(C1-C2)	0.3044	20.79	0.29	0.069
π(C13-C15)	1.66679	π*(C14-C16)	0.31432	19.79	0.29	0.068
		π*(C18-C20)	0.3229	19.95	0.29	0.068
π(C14-C16)	1.67129	π* (C13-C15)	0.34306	20.11	0.29	0.068
		π*(C18-C20)	0.3229	20.33	0.29	0.068
π(C18-C20)	1.66955	π(C14-C16)	0.31432	20.58	0.29	0.069
		π(C13-C15)	0.34306	20.13	0.29	0.068
LP1 O27	1.9738	σ*(C12-C26)	0.0936	23.56	0.61	0.109
LP2 O27	1.8413	σ*(C5-C6)	0.0164	33.98	0.66	0.136
LP2 O28	1.8028	σ*(C26-C27)	0.0231	52.89	0.35	0.123

The NBO analysis is also an efficient method for investigating charge transfer (CT) or hyperconjugative interaction in molecular systems. Some electron donor orbital, acceptor orbital and the interacting stabilization energies resulting from the second-order micro disturbance theory have been reported [20]. The larger the E(2) values, the more intensive is the interaction between electron donors and electron acceptors. The intramolecular hyperconjugative interactions are formed by the orbital overlap between π(C-C) and π*(C-C) bond orbitals which results intramolecular charge transfer (ICT) causing stabilization of the system. These interactions are observed as an increase in electron density (ED) in C-C antibonding orbital that weakens the respective bonds. The ED at the eight conjugated π bonds (~1.66–1.67 e) and π* bonds (~0.30–0.34 e) of the phenyl ring clearly demonstrate strong delocalization of electron leading to stabilization of (~19.5–20.7 kJ/mol) energy for the first and second ring. The other important interaction of BA are given in the Table 2.

4.3 Vibrational assignments

The experimental and theoretically predicted FT-IR and FT-Raman spectra for BA are shown in Figure 2 and 3. It is important to mention that the theoretical results refer to the isolated molecule in the gas phase, while comparisons were made with FT-IR and FT-Raman spectra of the solid sample. The calculated and observed IR and Raman wavenumber and their tentative assignment are given in the

Table 3. Comparison of the wavenumber calculated at the B3LYP with the experimental Table 3 reveals the overestimation of the calculated vibrational modes and is due to neglect of anharmonicity in the real system. Calculated wavenumbers were corrected by the linear scaling method. The calculated vibrational wavenumber at B3LYP level was scaled by 0.9670[14]. Comparison of the wavenumbers calculated by the DFT method using 6-311++G(d,p) basis set with experimental values shows a very a good agreement.

C–H vibrations

The heteroaromatic structure shows the presence of C–H stretching within the region 3000–3100 cm-1 which is the characteristic region for the ready identification of C–H stretching vibrations and typically exhibit weak bands compared with the aliphatic C–H stretching [23–25]. The weak to medium band observe in IR at 3072 and 3032 is assigned to C-H stretching vibration of the BA molecule. The same mode is observed in FT Raman at 3065, and 3039 cm-1. The aromatic C–H in-plane bending modes of benzene and its derivatives are observed in the region 1000–1300 cm-1 [26]. The series of bands observed in the FT-IR spectrum 1243, 1205, 1112, 1170 and 1054 1102 cm-1 FT-Raman spectrum 1217, 1189, 1137, 1103 and 1046 cm-1 are assigned to C–H in-plane bending vibrations of BA. From the table most of the theoretically computed scaled values by B3LYP method show a very good agreement with recorded data. The C–H out-of-plane deformation is observed between 1000 and 700 cm-1 [27]. Generally C–H out-of-plane deformation modes owned by highest wavenumbers have weaker intensity than those absorbing at lower wave numbers [27]. Accordingly in BA compound the C–H out-of-plane deformation are observed at 981 cm-1 in IR and 987 cm-1 in Raman.

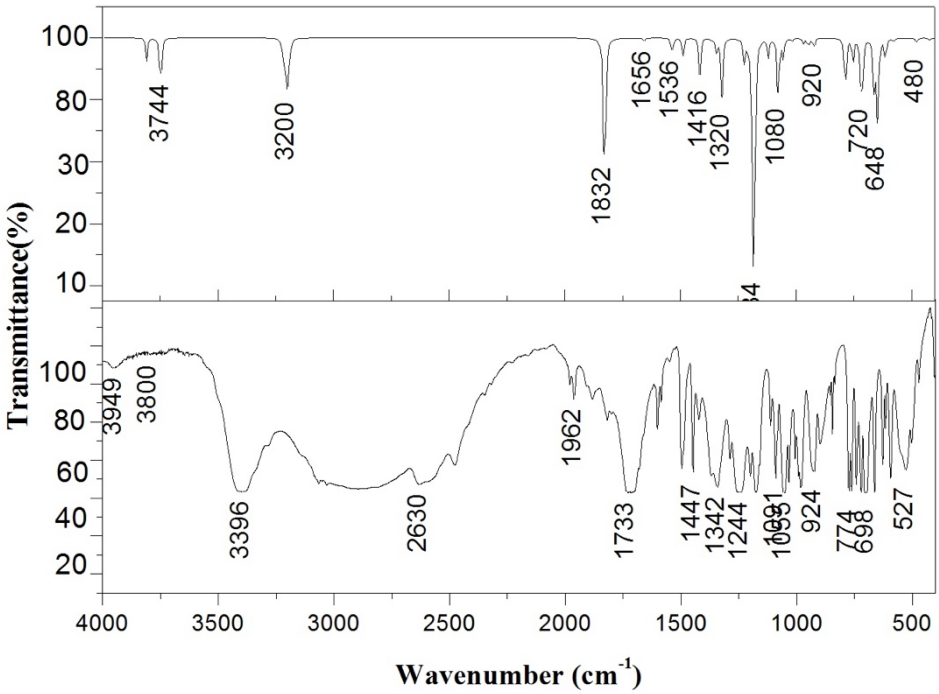

Figure 2: Combined IR spectra of Benzilic acid (a) FT-IR spectrum (b) Simulated IR spectrum.

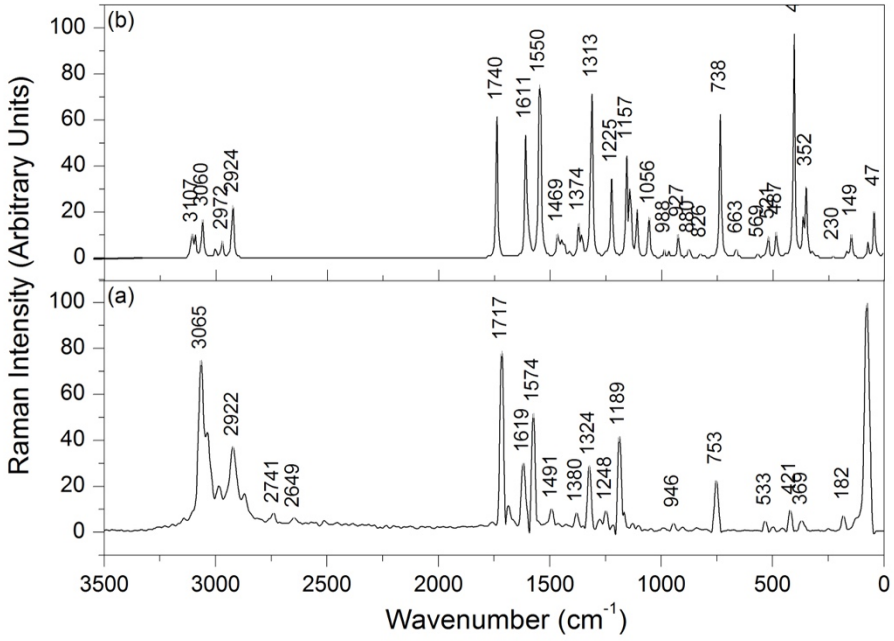

Figure 3:Combined Raman spectra of Benzilic acid (a) FT-Raman spectrum (b) Simulated Raman spectrum.

C–C vibrations

The ring C–C stretching vibrations are of variable intensity and give rise to characteristic bands in both the IR and the Raman spectra covering the spectral range from 1600 to 1400 cm-1 [28]. The observed bands in FT-IR at 1622, 1600, 1589 and 1495 cm-1 are assigned to C-C stretching mode of BA molecule. The same mode is observed in Raman at 1619, 1574 and 1491 cm-1. The above result shows that the ring C-C stretching vibration is simultaneously present in FT-IR and FT-Raman.

Table 3: Calculated and observed vibrational wavenumber and the tentative assignment of BA. Wave number (Scaled

Wave number (Scaled value)			**Assignments & PED%**
3736	-	-	$\nu O24$-$H25$(100%)
3679	-	-	$\nu O28$-$H29$(100%)
3229	3396 w	-	$\nu C15$-$H19$(94%)
3221	-	-	$\nu C1$-$H7$(83%)
3215	3281 m		$\nu C4$-$H9$+$\nu C4$-$H9$(84%)

3206	-	-	νC1-H7(91%)
3205	-	-	νC1-H7(92%)
3194	-	-	νC1-H7(85%)
3193	-	-	νC16-H21(91%)
3184	3072 s	3065vvs	νC16-H7(90%)
3183	3032 s	3039 w	νC16-H21(97%)
1831	1817 m		νC1-C2+βH7-C1-C6(51%)
1663	1701	1717 vvs	νO27-C26(87%)
1659	-	-	νC13-C14+βH19-C15-C13(60%)
1643	1622	-	νC1-C6(68%)
1640	1600	1619 m	νC2-C3(62%)
1546	1589	1574 s	C4-C5(67%)
1540	1553		βH17-C14-C13+νC1-C2(66%)
1496	1495	1491 w	βH7-C1-C6 +νC1-C2(57%)
1493	1447	1466 w	βH8-C2-C3(62%)
1422	1423	1421 w	βH25-O24-C12+νC12-C26(46%)
1373	-	1380 w	βH8-C2-C1 + νC1-C2(78%)
1365	-	-	βH17-C14-C16+νC14-C16(58%)
1349	1342	-	νC1-C2(58%)
1345	-		βH17-C14-C16+νC13-C14(45%)
1330	1326	1324 m	βH25-O24-C12(58%)
1228	1243	1248 m	νC20-O28(51%)
1223	-	-	βH7-C1-C6+νC1-C2(64%)
1214	-	1217 w	νC13-C14+βH19-C15-C13(56%) βH7-C1-C2
1195	1205	-	+νC1-C2(80%)
1194	-	-	βH19-C15-C18+νC3-C12(28%)
1192	-	1189 m	νC12-C26+βH19-C15-C18(47%)
1186	1177	-	βH25-O24-C12 +νC3-C12(26%)
1122	-	1137 w	νC14-C16+βH8-C2-C3(32%)
1121	1112	-	νC1-C2+βH7-C1-C6(57%)
1079	1097	1103 w	νO24-C12(48%)
1062	-	-	βH7-C1-C2 +νC1-C2(48%)
1057	1054	1046 w	βH17-C14-C13+νC1-C6(52%)
1020	1030	-	βC1-C6-C5 +νC1-C2(68%)
1019		-	βC13-C15-C18+νC13-C14(48%)
1001	1003	-	τH17-C14-C16-H21(87%)

997		987 w	τH7-C1-C6-H11(90%)
980	981	-	τH17-C14-C13-C12(86%)
970	-	-	τH7-C1-C2-H8(88%)
966	-	-	τH8-C2-C1-C6+νC12-C26(21%)
947	-	-	νC12-C26+ νC26-C12-O28-O27(12%)
936	-	946 w	τH8-C2-C1-C6(80%)
922	923	904 w	τH8-C2-C1-C6(58%)
868	900	-	τH17-C14-C16-C20(93%)
857	844	-	τH7-C1-C6-C5(95%)
792		-	τH7-C1-C2-C3+τC14-C13-C18*(28%)*
785	774	-	τH7-C1-C2-C3+τC14-C13-C18*(45%)*
756	748	753 m	γC26-C12-O28-O27+τH17-C14-C16-C20(48%)
722	-		τH17-C14-C16-C20+βC1-C6-C5(37%)
717	-		τH17C14C16C20+γC26C12O28O27(57%)
711	698		τH7-C1-C2-C3(66%)
663	660	676 w	τH29-O28-C26-C12+βC2-C1-C6(44%)
648	-	-	βC1-C6-C5+τH29-O28-C26-C12*(56%)*
634	-	-	βC2-C1-C6(84%)
633	633	-	βC-4C5-C6(86%)
615	610	-	τH29-O28-C26-C12(49%)
580	593	533 w	τC2-C1-C6-C5(54%)
504	527	499 w	τH19-C15-C13-C12(64%)
479	472		βC1-C6-C5+τC2-C1-C6-C5*(26%)*
423	-	421 w	τC1-C6-C5-C4+τC1-C6-C5-C4*(71%)*
414	-	-	τC1-C6-C5-C4*(76%)*
395	-	-	βC12-C13-C14(67%)
350	-	369 w	BC-4-C3-C12+νC12-C26*(44%)*
333	-	-	τC1-C6-C5-C4+τH29-O28-C26-C12*(44%)*
299	-	-	τH25-O24-C12-C26+βC1-C6-C5+νC3-C12*(27%)*
284	-	-	τH25-O24-C12-C26*(53%)*
270	-	252 w	βC4-C3-C12(73%)
245	-	-	τC14-C13-C15-C18+βC3-C12-C13*(39%)*
223	-	-	γC26-C3-C13-C12+βC4-C3-C12(43%)
141	-	182 w	βC3-C12-C13(69%)
106	-	-	γC26-C3-C13-C12*(79%)*

77	-	-	$\tau C3\text{-}C12\text{-}C13\text{-}C14+\beta C3\text{-}C12\text{-}C13(61\%)$
51	-	-	$\tau C3\text{-}C12\text{-}C26\text{-}O28(91\%)$
47	-	-	$\tau C3\text{-}C12\text{-}C13\text{-}C15+\beta C3\text{-}C12\text{-}C13(77\%)$
24	-	-	$\tau C2\text{-}C3\text{-}C12\text{-}C13(81\%)$

The simultaneous occurrence of C-C stretching mode is confirms the possibility of intramolecular charge transfer interaction of the BA molecule[29]. The possibility of intramolecular charge transfer interaction is already confirmed from the NBO analysis. From the table the theoretically scaled C–C stretching vibrations by DFT method show a good agreement with the recorded FT-IR and FT-Raman spectral shown in Table 3. The PED corresponding to all C–C stretching vibrations lies between 30% and 70% in combination with C–H in-plane bending and ring deformations. The bending vibrations of C-C mode is given in the Table 3.

Carbonyl vibrations

Normal esters are characterized by the strong IR absorptions due to the C O stretching vibration in the range 1750–1735 cm-1 and the C–O stretching vibration near 1200 cm-1. The unstrained, six-membered cyclic ester, δ-lactone absorbs at about the same value wavenumber as a noncyclic ester. The conjugated ester part gives an intense IR band at 1720 cm-1[30]. In BA, the O27 is conjugated with C12-C20 and O24 is conjugated with C12-C13 double bonds. In the BA molecule carbonyl stretching vibration is observed in IR and Raman as a very strong band at 1701 and 1717 cm-1 respectively. It confirms the conjugated carbonyl group present in the molecule. This conjugative carbonyl leads the hyperconjugation interaction with increase in the single bond character. The O1-C6 stretching vibration is observed as a medium in IR and Raman at 1243 and 1248 cm-1 respectively. The single bond C-O is observed as medium band in comparison with the C=O is due to C-O is less characteristic in nature and is sensitive to substitution. The in-plane and out-of-plane bending of the carbonyl group is mixed significantly with the in-plane and out-of-plane bending vibrations of C-C and **C-H vibration.**

4.4 Mulliken and Natural population analysis

The natural atomic charge has an important role in the application of quantum mechanical calculation for the molecular system. The natural population analysis of BA obtained by Mulliken [34] and natural population analysis with B3LYP level using 6-311++G(d,p). B3LYP/6-311+G(d,p) method as shown in Figure 4. From the table 4 all the carbon and oxygen atoms are negatively charge except C3, C12 and C13 and all the hydrogen atoms are positively charge. Atom O24 is largely negative than oxygen atoms is due to the possibility of charge transfer from O24to the ring. The atomic charge analysis shows that the substitution of the methyl will redistribute electronic charge over the ring system as evident from the C13=0.0861e in the mulliken analysis whereas C13=-0.2478in the natural population analysis.

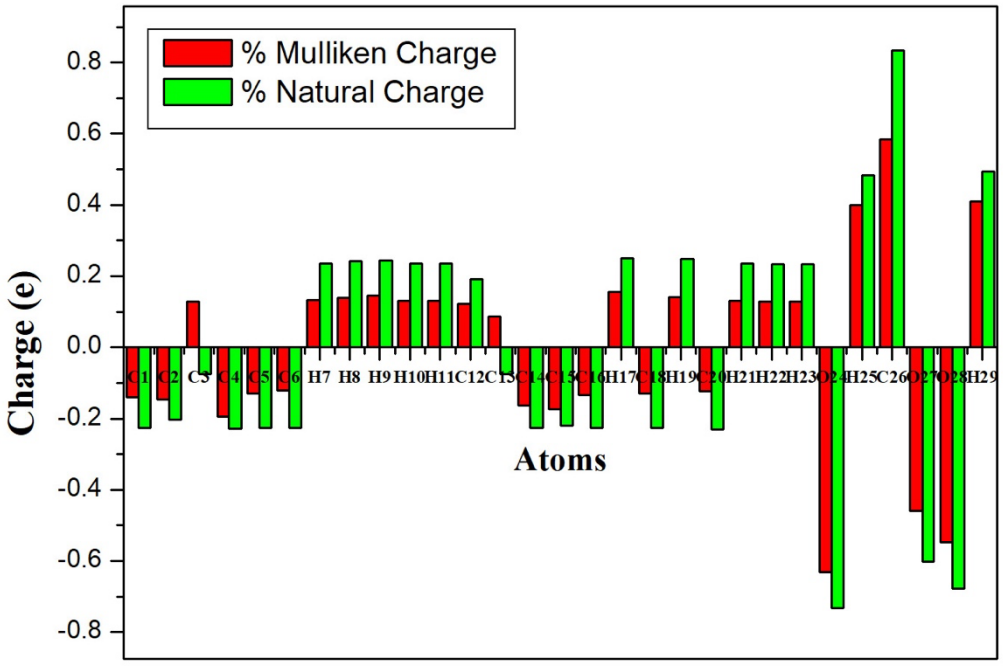

Figure 4: Mulliken and Natural charge plot of BA.

Table 4. Mulliken and Natural charge of Benzilic acid calculated at DFT level.

Atoms	Mulliken Charge (e)	Natural Charge (e)
C1	-0.1395	0.2366
C2	-0.1458	0.2411
C3	0.1286	0.2452
C4	-0.1954	0.2357
C5	-0.1308	0.235
C6	-0.1212	0.1921
H7	0.1325	-0.0753
H8	0.1384	-0.2259
H9	0.1453	-0.2201
H10	0.131	-0.2262
H11	0.1304	0.251
C12	0.1234	-0.2254
C13	0.0861	0.2478
C14	-0.1629	-0.2304
C15	-0.1745	0.236
C16	-0.1351	0.2346

H17	0.1553	0.2341
C18	-0.1296	-0.733
H19	0.1409	0.4831
C20	-0.1227	0.8335
H21	0.1314	-0.603
H22	0.1292	-0.6782
H23	0.1284	0.2366
O24	-0.6313	0.2411
H25	0.4001	0.2452
C26	0.5845	0.2357
O27	-0.4597	0.235
O28	-0.5474	0.1921
H29	0.4103	-0.0753

4.5 Molecular electrostatic potential

Molecular electrostatic potential (MESP) at a point in the space around a molecule gives an indication of the net electrostatic effect produced at that point by the total charge distribution (electron + nuclei) of the molecule and correlates with dipole moments, electronegativity, partial charges and chemical reactivity of the molecule. It provides a visual method to understand the relative polarity of the molecule. An electron density isosurface mapped with electrostatic potential surface depicts the size, shape, charge density and site of chemical reactivity of the molecule. Such mapped electrostatic potential surface has been plotted for the title molecule in 6-31G(d,p) basis set using the computer software Gauss view [13]. A projection of this surface along the molecular plane is given in Figure 5.

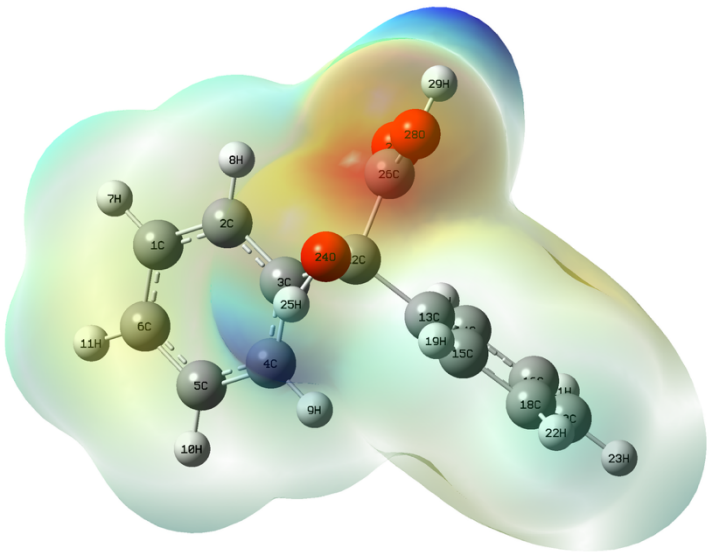

Figure 5: Molecular electrostatic plot of BA

The different values of the electrostatic potential at the surface are represented by different colors: red represents regions of most negative electrostatic potential, blue represents regions of most positive electrostatic potential and green represents regions of zero potential. Potential increases in the order: red < orange < yellow < green < blue. In all cases, the shape of the electrostatic potential surface is influenced by the structure and charge density distributions in the molecule with sites close to the oxygen atom, showing regions to most of the negative electrostatic potential. The calculated 3D MEP shows the negative regions are electrophilic region, these are mainly due to O24, O27 and O28 atoms. The positive regions are the nucleophilic region and these are over the hydrogen atoms of the title molecule BA. It shows that the potential has been used primarily for predicting sites and relative reactivities towards electrophilic attack and in studies of pharmaceutical recognition and hydrogen bonding interactions [35, 36].

4.6 HOMO, LUMO analysis:

HOMO-LUMO analysis is a quantum mechanical method that uses the highest occupied molecular orbital (HOMO) and the lowest unoccupied molecular orbital (LUMO) to predict a molecule's chemical reactivity, stability, and electronic properties[37-40]. A large HOMO-LUMO energy gap indicates high stability and low reactivity, while a small gap suggests lower stability and higher reactivity, with the gap also correlating to optical absorption properties and charge transfer behavior. This analysis is used in fields like materials science, drug design, and organic electronics to design molecules for specific applications [41-43]. The spatial plot of HOMO-1, HOMO, LUMO and LUMO + 1 orbitals are illustrated in Figure 6. The corresponding energy Eigen values and HOMO-LUMO gap are presented in Table 5. The HOMO is delocalized over all atoms while the LUMO is delocalized over the whole molecule except the methyl group. The density plot of HOMO and LUMO shows the charge transfer from the methyl group to through the ring within molecule upon excitation at lowest excitation energy (3.9180 eV). These frontier molecular orbitals explain the way the molecule interacts with another chemical species. The HOMO-LUMO gap is an important parameter that estimates the chemical stability, reactivity and electron conductivity. The HOMO, LUMO energy and HOMO–LUMO energy gap of BA was calculated at the B3LYP/6-311++G(d,p) level. The HOMO and LUMO energy of BA is found to be -5806 eV, -4.6087 eV. The HOMO–LUMO energy gap is found to be 4.9719 eV. The calculated energy gap is comparatively small and it explains the eventual charge transfer interaction within the molecule, which influences the anticoagulants activity of the molecule. Consequently, the lowering of the HOMO–LUMO band gap is essentially a consequence of the large stabilization of the LUMO due to the strong electron-acceptor ability of the electron-acceptor group. This low gap also suggests an easy electronic transition as well as its high reactivity.

Table 5. Global Reactivity descriptors of Benzili zcid

Molecular Properties	Mathematical Description	Energy(eV)
E_{HOMO}	Energy of HOMO	-9.6087

E_{LUMO}	Energy of LUMO	-4.5806
Energy Gap	$\Delta E_g = E_{HOMO} - E_{LUMO}$	4.9719
Ionization Potential (I_P)	$IP = - E_{HOMO}$	9.6087
Electron Affinity (E_A)	$EA = - E_{LUMO}$	4.5806
Electronegativity (χ)	$\chi = - 1/2(E_{LUMO} + E_{HOMO})$	7.0946
Chemical potential (μ)	$\mu = 1/2(E_{LUMO} + E_{HOMO})$	-7.0946
Global Hardness (η)	$\eta = 1/2(E_{LUMO} - E_{HOMO})$	2.5140
Softness (S)	$S = 1/2\eta$	1.257
Electrophilicity index (ω)	$\omega = \mu^2/2\eta$	9.990

The HOMO energy characterizes the susceptibility of the molecule toward attacks by electrophiles while the LUMO energy describes the susceptibility of the molecule toward attacks by nucleophiles. The global chemical reactivity descriptors like ionization potential, electro affinity, electronegativity, chemical potential, electrophilicity, hardness and softness based on HOMOLUMO energy values were also computed and depicted in Table 5. The important role of DFT based chemical reactivity indices mainly electrophilicity and ionization potential is to predict chemical nature in prediction of biological activities. The electrophilicity descriptor for the present compound is found to be 9.90 eV which suggests that this compound to be a good electrophile. The higher electrophilicity index value, indicates that it can act as an electrophilic species and has a greater ability to bind to pharmaceutical[44]. The Global hardness (η) and Chemical potential (μ) values are calculated as 2.5140and -7.0946respectively. The title compound is a soft compound with strong polarizability, as indicated by the lower global hardness value and high negative chemical potential [45].

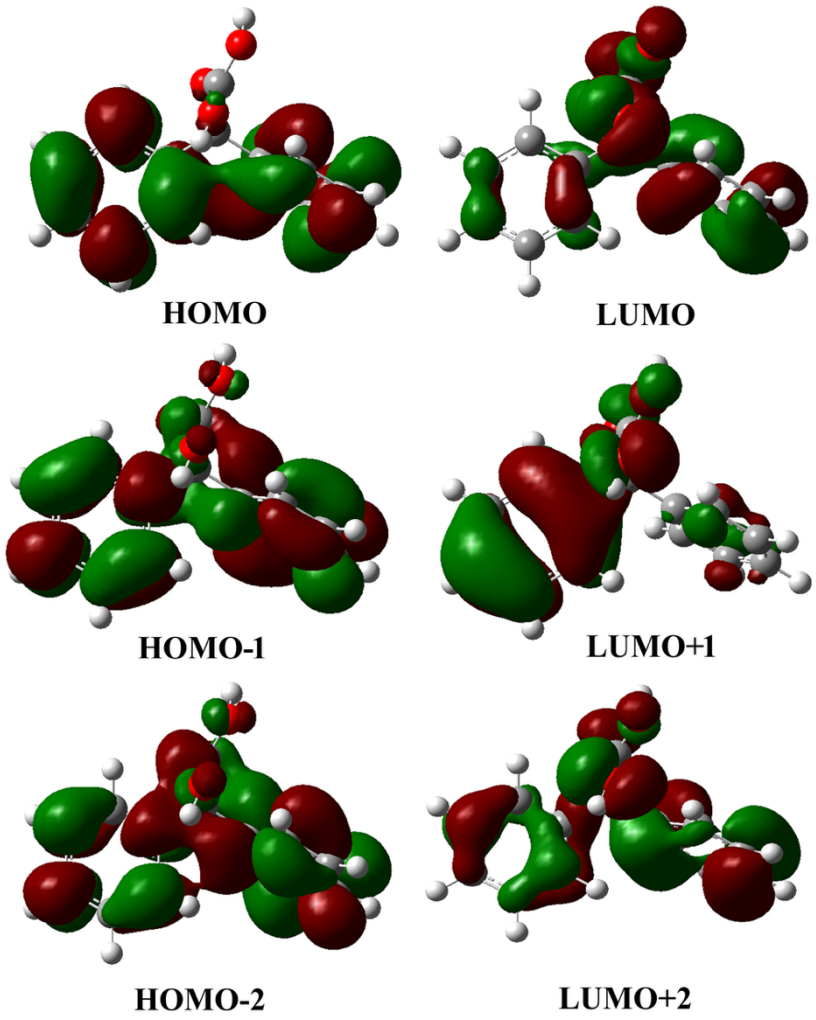

Figure 6:HOMO LUMO plot of BA calculated at DF level

4.7. Chemical bonding analysis

As per the Becke and Edgecombe [46] the impetus for a density-based description of chemical bonding led to the development of new descriptors such as the electron localization function (ELF) introduced by localized-orbital locator (LOL) [47,48], These methods are mainly based on topological methods. Because the reduction of the quantum kinetic-energy density by orbital sharing is the driving force of covalent bonding and the kinetic energy density serves as the central property on which the position descriptors are centred. [49,50]. Consideration of the electron pair density is the foundation of ELF while LOL simply recognizes that, gradients of localized orbitals are maximized when localized orbitals overlap.

4.7.1 Electron localization function (ELF)

Electron localization is an important parameter to explain the aromaticity of a molecule, the nature of chemical bonding in transition metal complexes [51] and most importantly it directly reveals the Pauli

exchange repulsion effect by measuring the excess of local kinetic energy due to Pauli repulsion which has several applications in VSEPR theory [52]. This leads to a deformation of the ELF distribution around the oxygen atom of the carbonyl group as observed in figure 7. By examining ELF values of oxygen along with the carboxylic acid group, values are lower (represented by blue).The electrons in the bonds between the carbon-carbon atoms showed localization (represented by red region) in comparison to the electrons in the bonds between carbon-hydrogen (represented by green region).

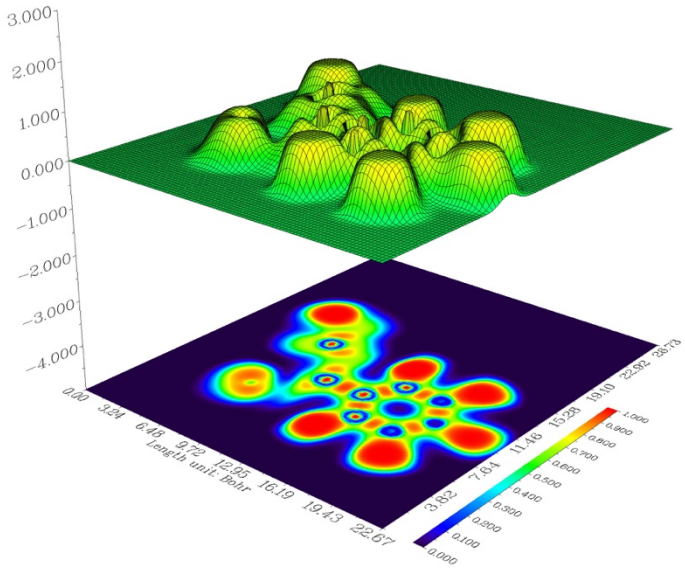

Figure 7 : 2D plot electron localization function isosurfaces with projection for Benzilic acid

4.7.2 Localized orbital locator (LOL)

Molecular orbitals which are concentrated in a limited spatial region constitute the localized molecular orbitals. Figure 8 shows its localized orbital locator (LOL) distribution under 6-311G (d,p) basis set. For the title compound, the blue colour corresponds to low values of LOL some of carbon and hydrogen and S atoms present in the positive region and it indicates a blue in colour. The blue represents the region with the low end of LOL value of other lowest attraction atoms that are surrounded by yellow region.

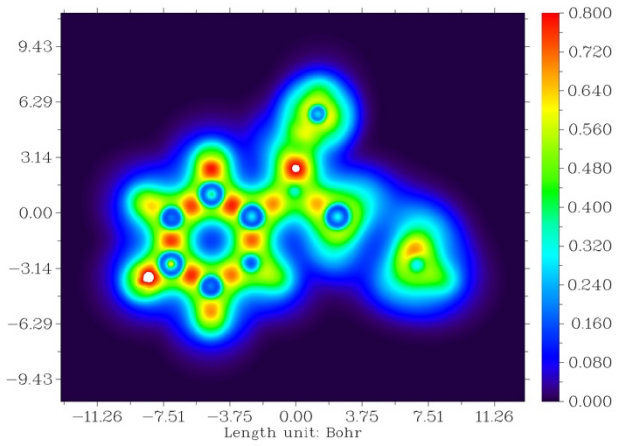

Figure 8 . Relief map with projection of localized orbital locator of Benzilic acid

4.7.3 AIM Analysis

Atoms in molecule(AIM) is a powerful method to gather knowledge about the chemical bonding and hydrogen bondings in the molecular system[53-54]. The important interaction such as (i) for strong H-bonds (2ρBCP) <0, HBCP < 0 and covalent in nature, (ii) for medium H-bonds (2ρBCP) > 0, HBCP < 0 and partially covalent in nature and (iii)for weak H-bonds (2ρBCP) > 0 and HBCP > 0 and electrostatic in nature can be identified from topological analysis of the electronic charge density and their Laplacian at the bond critical point (BCPs). The AIM analysis has obtained the electron density region and calculates the properties of BCPs. If the electron density is higher, then it shows that bond is stronger. Negative value of 2ρ represents the covalent nature at the BCP of the covalent bond, the electron density is concentrated in the region between the interrelate atoms, thus creating a common electron pair, which is considerably localized. Positive values of 2ρ estimated at the corresponding BCP indicate closed-shell interactions where depletion of electronic charge along the bond path occurs which is characteristic of closed shell interactions such as hydrogen bonds. The bond ellipticity Ɛ, has been examined as a revealing measure of the pi-bond character and also defines the cycle susceptibility to opening. Larger the value of ellipticity and the larger will be the pi delocalization.

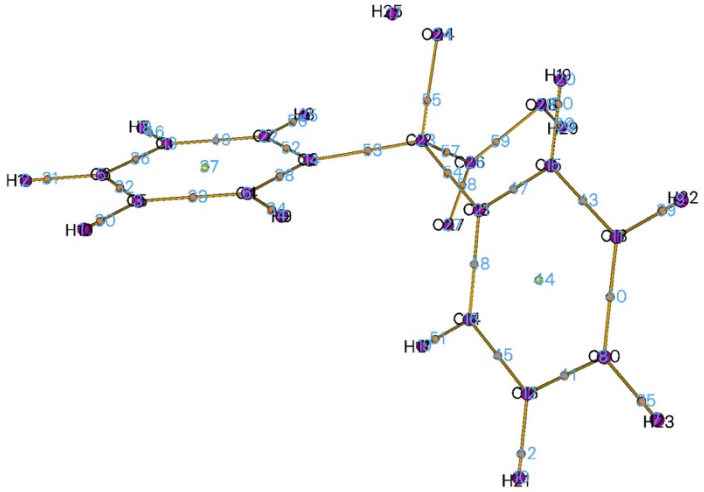

Figure 9: Bond Critical Points And Ring Critical Points in AIM analysis

Table 6 : Topological Parameters:Electron density (ρ), Laplacian of Electron density (∇2ρ), Ellipticity at bond critical point (BCP).

Name	Atoms	Rho(ρ)	□2ρ	Ellipticity
BCP1	C1-C2	0.3527	-0.7430	0.0027
BCP2	C2-C3	0.3523	-0.7417	0.0027
BCP3	C3-C4	0.9374	-0.7394	0.000042
BCP4	C4-C5	0.3517	-0.7386	0.0026
BCP5	C5-C6	0.9374	-0.7394	0.000040
BCP6	C1-C7	0.9376	-0.7396	0.000042
BCP7	C2-H8	0.3523	-0.7417	0.0028
BCP8	C4-H9	0.9374	-0.7394	0.000038
BCP9	C5-H10	0.3527	-0.7431	0.0027
BCP10	C6-H11	0.3528	-0.7431	0.0027
BCP11	C3-C12	0.9374	-0.7394	0.000042
BCP12	C12-C13	0.9374	-0.7394	0.000042
BCP13	C13-C15	0.9374	0.7394	0.000042
BCP14	C14-C16	0.9366	-0.7389	0.000043
BCP15	C14-H17	0.9376	-0.7396	0.000039
BCP16	C15-C18	0.9376	-0.7396	0.000039

BCP17	C15-H19	0.3074	-0.5121	0.0060
BCP18	C18-C20	0.3527	-0.7428	0.0027
BCP19	C19-N20	0.3515	-0.7385	0.0027
BCP20	C16-H21	0.3529	-0.7414	0.000028
BCP21	C18-H22	0.9372	-0.7394	0.000045
BCP22	C20-H23	0.9375	-0.7396	0.000041
BCP23	C12-O24	0.9380	-0.7408	0.000039
BCP24	O24-H25	0.2330	-0.3375	0.000081
BCP25	C12-C26	0.3530	-0.7424	0.002683
BCP26	C26-O27	0.9333	-0.7358	0.000055
BCP26	C26-O28	0.2333	-0.3381	0.000015
BCP26	O28-H29	0.2330	-0.3375	0.000078

From the AIM analysis electron density ρ, its Laplacian density and the ellipticity have been calculated and the parameters for the title compound is tabulated in Table 6. The critical points and their corresponding plot obtained by B3LYP/6-311++G(d,p) method using multiwfn program are shown in Figure 9. In the ba molecule, the electron density is maximum for C12-O24 (0.938), C1-C7(0.9376), C14-H17, C15-C18 (0.9376), bond and these bonds have a greater negative value of 2ρ showing its covalent nature. In ellipticity the C15-C19 atom shows higher value than others and it indicates the nonstability of the bond.

4.7.5 Reduced density gradient (RDG) analysis

The Reduced Density Gradient(RDG) is a fundamental dimensionless quantity coming from the density and its first derivative:

$$RDG(r) = \frac{1}{2(3\pi r^2)^{1/2}} \frac{|\nabla \rho(r)|}{\rho(r)^{4/3}} \quad \text{……..(4.2)}$$

The real space weak interaction is based on electron density and RDG analysis developed by Johnson et al. [46]. From Figure 10 and 11 the weak interaction is identified by analyzing the below electron density values. The plot of RDG vs r provides the presence of interaction strength. The λ2 sign is used to differentiate the bonding ($\lambda 2 < 0$) interactions from non- bonding ($\lambda 2 > 0$) interaction. The Multiwfn and VMD software analyze the interaction of strength in the molecular system, in which blue color indicates stronger attraction and red indicates repulsion. From shown, the red color represents the ring system which is responsible for the steric effect. In this molecule, the steric effect is more which is represented in red color in the RDG scatter plot.

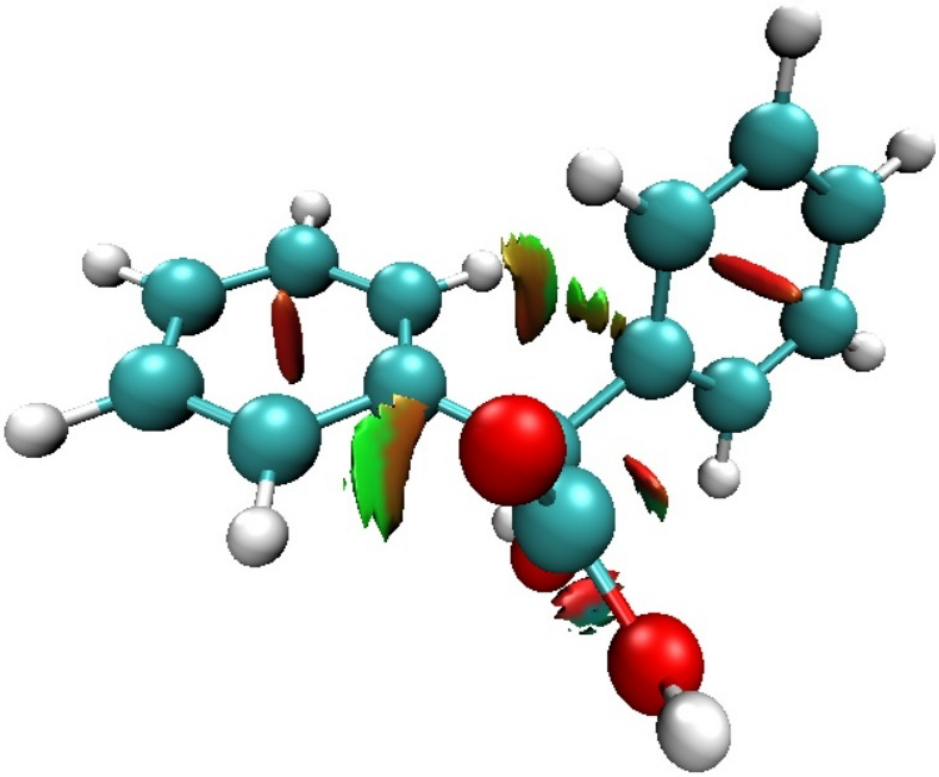

Figure 10. Plots of the NCI of BA

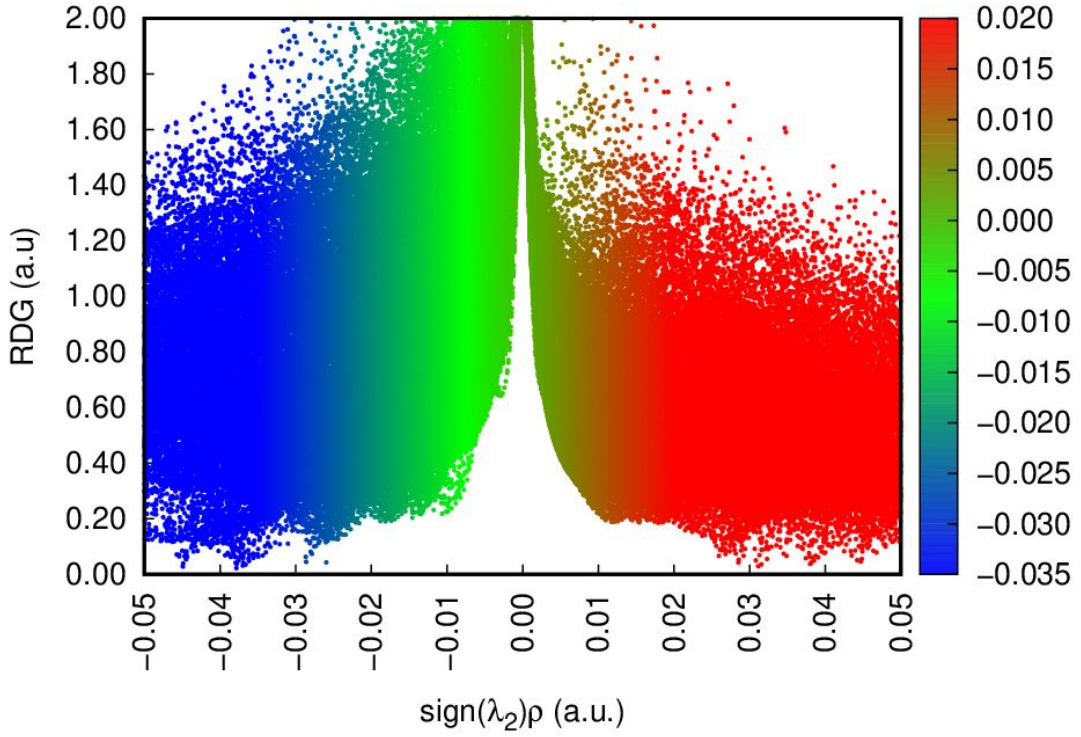

Figure 11. Plots of the RDG versus the electron density ρ multiplied by the sign of λ2 for BA

4.8. Drug likeness:

Drug-likeness isone of the most significant variables in the early phases of drug discovery. Drug likeness a qualitative property of chemicals that describes how closely a compound's qualities resemble those of already-approved drugs [55].The most popular way to judge druglikeness is through rules, the most well-known of which is Lipinsk's Rule of Five (Ro5) [56]. The relationship between physicochemical and pharmacokinetics indices is illustrated by this rule-of-five[57].According to Lipinski's rule, an orally active drug-like compound cannot violate more than one of the following conditions: its molecular weight shouldn't exceed 500 Da, its hydrogen bond donors shouldn't exceed 5, its hydrogen bond acceptors shouldn't exceed 10, its molar refractivity should lie between 40-130, and its log P shouldn't exceed 5 [58]. A few key variables, including the compound's rotatable bonds, logP, molar refractivity, hydrogen bond acceptors (HBA) and donors (HBD) numbers, are utilised to determine the drug-likeness quality of the molecule [59]. The drug likeness properties are calculated by using the Swiss ADME software and the obtained results are organized in table 7.

Table 7. Drug likeness parameters of the title compound.

Descriptors	Calculated	Expected
Molecular mass (Dalton)	228.24	<500
Hydrogen bond donor	2	<5
Hydrogen bond acceptor	3	<10
Log P	1.19	<5
Molar refractivity	63.52	40–130

For title compound, the Molecular mass is calculated as 228.24Da. The hydrogen bond donors and acceptors are calculated as 2 and 3 respectively. The molar refractivity is calculated as 63.52. The log P value is obtained as 1.19which is analysed to be within the suitable range. From the drug likeness results, the title compound complies with Lipinski's rule of five with no violations and it can be used as an active prospective drug. It is also confirmed from the docking results, as the title compound has high binding affinity (-6.1 kcal/mol) towards the antimalarial protein and exhibits good antimalarial activity.

44.9 Molecular docking

Molecular docking provides insight into plausible protein ligand interactions. Docking was done to find the best orientation of ligand which would form a complex with overall minimum energy. The optimized structure of BA obtained from Gaussian '09 [15] using the B3LYP/6-311++G(d,p) level was docked using AUTODOCK 4.2 docking software with the structures of protein retrieved from PDB [36] (PDB ID-1COU, 1MH0). The crystal structures of the above receptors [60, 61], were obtained from PDB. AUTODOCK 4.2 docking software is an algorithm for docking ligands into protein binding sites. Docking was constrained to the above mentioned sites, which are established potent binding sites for BA, thereby reducing the necessity for extensive search. One hundred independent docking runs were carried out for each ligand, and results differing by less than 1.5 Å in positional root mean-square deviation (rmsd) were clustered together and represented by the result with the most favorable free energy of binding to give a top-ranked cluster (2V9P and 3W6G) as shown in Figure 12 and 13., which proved to fit most excellently. Amine acids present in the active site of 2V9P and 3W6G, is attached to the oxygen atom of benzilic acid of drug by forming C-H…..O hydrogen bonding indicated by dashed lines. The selected protein used as a anticoagulants activity. Our ligand BA perfectly docked with the target anticoagulants(2V9P and 3W6G). It confirms anticoagulant activity of the molecule BA. In the docking analysis the ligand was linked with the protein through the C-H…O hydrogen bond and therefore the C-H….O hydrogen bonding and the Oxygen atom of coumarin molecule is the responsible for the anti tumor and anti oxidant activity of the molecule.

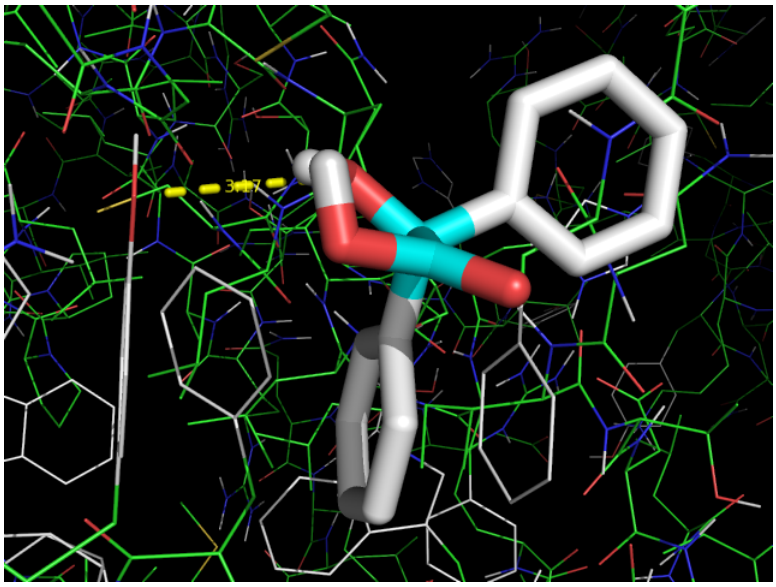

Figure 12: Benzilic acid ligand bind at the active site of 2V9P anti tumer target protein

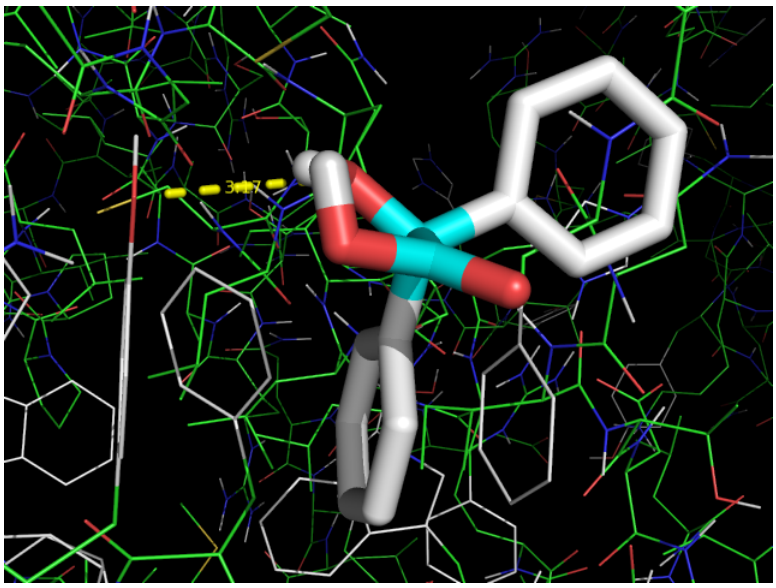

Figure 12: Benzilic acid ligand bind at the active site of 3W6G anti oxidant target protein

5. Conclusion

Using the quantum chemical computations, the structural, vibrational and topological characteristics of the compound was studied. The 6-311++G(d,p) basis set was used to optimise the Molecular geometry employing DFT-B3LYP and the structural parameters were identified. The intra- and inter-molecular interactions calculated from the NBO analysis confirms the bioavailability of the compound. The HOMO-LUMO energy values and the global reactivity descriptors were also calculated. The HOMO-LUMO energy gap is calculated as 4.9719 eV which also accounts for the biological activity

of the molecule.The vibrational spectra were thoroughly interpreted with the aid of VEDA software. FT-IR and FT-Raman spectra have recorded and the values agreed with the theoretical vibrational assignments. The steric repulsion,weak and strong attractions of the tile compound was analysed by using the NCI approach. MEP and the topological analysis like ELF, LOL, AIM etc, were utilised to evaluate the title compound's reactive sites and electron distribution. The drug likeness studies strengthens that the title compound can be utilised as an active medication to treat specific illnesses. For the molecular docking studies, the target protein is docked with antitumor and anti oxidant target proteins. Among them the title compound has high binding affinity (-6.4 and -5.8 kcal/mol) towards the antitumor and anti oxidant protein and exhibits good antitumor and anti oxidant activity.

Reference:

[1] Shu-Feng Zhao, Huan Wang, Yang-Chan Lan and Xiao Liu, Journal of Electroanalytical Chemistry, 664 105-110 2012
[2] I B Gozlan, J. Heterocycl. Chem. 19 1569 1982
[3] E Hannig, Pharmazie, 34 670 1971
[4] R Harold, Nace, X David and Nelander, J. Org. Chem. 7 29 1964
[5] Volkan Cicek, Mehmet Ozdemir, Allen W Apblett, International Journal of Chemistry, 5 1 2013
[6] O Seiler, M Penka and R Tacke, Inorg. Chim. Acta 357 1955 2004
[7] M S Chen, D Z Kuang and C H Zhang, Chinese J. Struc. Chem. 24 1249 2005
[8] Y Q Yang and Y F Kuang, Chinese J. Inorg. Chem. 22 303 2006
[9] Yongcai Qiu, Kunnan Wang, Yan Liu, Hong Deng , Feng Sun and Yuepeng
[10] R.K. Raj, S. Gunasekaran, T. Gnanasambandan , S. Seshadri Combined spectroscopic and DFT studies on 6-bromo-4-chloro-3-formyl coumarin, Spectrochimica Acta Part A: 139 (2015) 505–514
[11] M.J. Frisch, G.W. Trucks, H.B. Schlegel, G.E. Scuseria, M.A. Robb, J.R. Cheeseman, G. Scalmani, V. Barone, B. Mennucci, G.A. Petersson, H. Nakatsuji, M. Caricato, X. Li, H.P. Hratchian, A.F. Izmaylov, J. Bloino, G. Zheng, J.L. Sonnenberg, M. Hada, M. Ehara, K. Toyota, R. Fukuda, J. Hasegawa, M. Ishida, T. Nakajima, Y. Honda, O. Kitao, H. Nakai, T. Vreven, J.A. Montgomery Jr., J.E. Peralta, F. Ogliaro, M. Bearpark, J.J. Heyd, E. Brothers, K.N. Kudin, V.N. Staroverov, R. Kobayashi, J. Normand, K. Raghavachari, A. Rendell, J.C. Burant, S.S. Iyengar, J. Tomasi, M. Cossi, N. Rega, J.M. Millam, M. Klene, J.E. Knox, J.B. Cross, V. Bakken, C. Adamo, J. Jaramillo, R. Gomperts, R.E. Stratmann, O. Yazyev, A.J. Austin, R. Cammi, C. Pomelli, J.W. Ochterski, R.L. Martin, K. Morokuma, V.G. Zakrzewski, G.A. Voth, P. Salvador, J.J. Dannenberg, S. Dapprich, A.D. Daniels, O. Farkas, J.B. Foresman, J.V. Ortiz, J. Cioslowski, D.J. Fox, Gaussian 09, Revision A.02, Gaussian, Inc., Wallingford CT, 2009.
[12] H. Arslan, O. Algul, T. Onkol, Vibrational spectroscopy investigation using ab initio and density functional theory analysis on the structure of 3-(6-benzoyl-2-oxobenzo[d]oxazol-3(2H)-yl)propanoic acidSpectrochim. Acta A 70 (2008) 606-614.

[13] R.I. Dennington, T. Keith, J. Millam, K. Eppinnett, W. Hovell, Gauss View, Version 3.09, Semichem, Inc., Shawnee Mission, KS, 2003.
[14] A.P. Scott, L. Radom, Harmonic Vibrational Frequencies: An Evaluation of Hartree−Fock, Møller−Plesset, Quadratic Configuration Interaction, Density Functional Theory, and Semiempirical Scale Factors J. Phys. Chem. 100 (1996) 16502-16513.
[15] H. Jamroz, Vibrational Energy Distribution Analysis VEDA 4, Drug Institute, Warsaw, Poland, 2004.
[16] G. Keresztury, S. Holly, J. Varga, G. Besenyei, A.Y. Wang, J.R. Durig, Vibrational spectra of monothiocarbamates-II. IR and Raman spectra, vibrational assignment, conformational analysis and ab initio calculations of S-methyl-N,N-dimethylthiocarbamate, Spectrochim. Acta, Part A 49 (1993) 2007-2017.
[17] G. Keresztury, J.M. Chalmers, P.R. Griffith, Raman Spectroscopy: Theory in Handbook of Vibrational Spectroscopy, vol. 1, John Wiley & Sons Ltd, New York, 2002.
[18] Ligia R. Gomes, John Nicolson Low, Andre Fonseca, Maria Joao Matos and Fernanda Borges Acta Crystallographica Section E, 72 (2016) 926-932
[18] I. Hubert Joe, Irena Kostova, C. Ravikumar, M. Amalanathan and Simona Cînt ˇa Pînzaru Theoretical and vibrational spectral investigation of sodium salt of acenocoumarol, J. Raman Spectrosc. 2009, 40, 1033–1038.
[19] E.D. Glendening, J.K. Badenhoop, A.E. Reed, J.E. Carpenter, J.A. Bohmann, C.M. Morales, F. Weinhold, NBO 5.0, Theoretical Chemistry Institute, University of Wisconsin, Madison, 2001.
[20] F. Weinhold, A new twist in molecular shape, Nature 411 (2001) 539-541.
[21] A.E. Reed, L.A. Curtiss, F. Weinhold, Intermolecular interactions from a natural bond orbital, donor-acceptor viewpoint, Chem. Rev. 88 (1988) 899-926.
[22] Adel A. El-Azhary, Joseph S. Alper, Marian A. Lowe, Timothy A. Keiderling, Spectrochim. Acta A, 44, (1988) 1315-1326.
[23] V. Krishnakumar, R. John Xavier, Normal coordinate analysis of 2-mercapto and 4,6-dihydroxy-2-mercapto pyrimidinesIndian J. Pure Appl. Phys. 41 (2003) 597.
[24] J. Coates, in: R.A. Meyers (Ed.), Interpretation of Infrared spectra, A Practical Approach, John Wiley and Sons Ltd., Chichester, 2000.
[25] E. Tasal, I. Sidir, Y. Gulselvan, C. Ogretir, T. Onkol, Vibrational spectra and molecular structure of 3-(piperidine-1-yl-methyl)-1,3-benzoxazol-2(3H)-one molecule by density functional theory and Hartree–Fock calculations, J. Mol. Struct. 923 (2009) 141.
[26] M. Amalanathan,I. Hubert Joea and Irena Kostova, Density functional theory calculation and vibrational spectral analysis of 4-hydroxy-3-(3-oxo-1-phenylbutyl)-2H-1-benzopyran-2-one, J. Raman Spectrosc. 2010, 41, 1076–1084.
[27] V. Arjunan, K. Carthigayan, S. Periandy, K. Balamurugan, S. Mohan, Quantum chemical studies and vibrational analysis of 4-acetyl benzonitrile, 4-formyl benzonitrile and 4-hydroxy benzonitrile – A comparative study, Spectrochim. Acta A, Mol. Biomol. Spectrosc. 98 (2012) 156–169.

[28] S. Jeyavijayan, M. Arivazhagan, FTIR and FT-Raman spectra, molecular geometry, vibrational assignments, first-order hyperpolarizability, ab initio and DFT calculations for 3,4-dimethoxybenzonitrile, Spectrochim. Acta A, Mol. Biomol. Spectrosc. 81 (2011) 466–474.
[29]. M. Amalanathan, I. Hubert Joe, and S. S. Prabhu Charge Transfer Interaction and Terahertz Studies of a Nonlinear Optical Material l-Glutamine Picrate: A DFT Study, J. Phys. Chem. A 2010, 114, 13055–13064.
[30] D. Sajan, I. Hubert Joe, V.S. Jayakumar, NIR-FT Raman, FT-IR and surface-enhanced Raman scattering spectra of organic nonlinear optic material: p-hydroxy acetophenone, J. Raman Spectrosc. 37 (2005) 508.
[31] M. Gussoni, C. Castiglioni, M.N. Ramos, M.C. Rui, G. Zerbi, Infrared intensities: from intensity parameters to an overall understanding of the spectrum J. Mol. Struct. 224 (1990) 445-470.
[32] L. Padmaja , M. Amalanathan, C. Ravikumar, I. Hubert Joe, NBO analysis and vibrational spectra of 2,6-bis(p-methyl benzylidene cyclohexanone) using density functional theory Spectrochimica Acta Part A 74 (2009) 349–356
[33] R.S. Mulliken, Electronic Population Analysis on LCAOMO Molecular Wave Functions, J. Chem. Phys. 23 (1995) 1833–1840.
[34] P. Politzer, J.S. Murray, Electrostatic potential analysis of dibenzo-p-dioxins and structurally similar systems in relation to their biological activities, in: D.L. Beveridge, R. Lavery (Eds.), Theoretical Biochemistry and Molecular Biophysics: A Comprehensive Survey, Protein, vol. 2, Adenine Press, Schenectady, NY, 1991 (Chapter 13).
[35] P. Politzer, D.G. Truhler (Eds.), Chemical Applications of Atomic and Molecular Electrostatic Potentials, Plenum Press, NY, 1981.
[36] L.Q. Chai, H.S. Zhang, W.K. Dong, Y.L. Zhao, Synthesis of unsymmetrical ureas with coumarin and thiadiazole under microwave irradiation, Phosphorus, Sulfur, Silicon Rel. Elem 185 (2010) 1332-1337.
[37] L.Q. Chai, H.S. Zhang, Y.L. Zhang, K. Cui, Synthesis of asymmetric semicarbazides using a coumarin ring, J. Chem. Res. 36 (2012) 12-14.
[38] H.O. Kalinowski, S. Berger, S. Braun, Carbon 13 NMR Spectroscopy, John Wiley and Sons, Chichester, 1988.
[39] K. Pihlajer, E. Kleinpeter, Carbon 13 Chemical Ahifts in Sructural and Streo Chemical Analysis, VCH Publishers, Deerfield Beach, 1994.
[40] M.K. Paria, J. Dinda, T.H. Lu, A.R. Paital, C. Sinha, Zn(II), Cd(II) and Hg(II) complexes of 8-aminoquinoline.Structure, spectra and photoluminescence property, Polyhedron 26 (2007) 4131e4140.
[41] C. Adamo, D. Jacquemin, The calculations of excited-state properties with time-dependent density functional theory, Chem. Soc. Rev. 42 (2013) 845e856
[42] Alasdair T.R. Laurie, Richard M. Jackson, Q-SiteFinder: an energy-based method for the prediction of proteineligand binding sites, Struct. Bioinforma. 21 (2005) 1908.
[43] https://www.rcsb.org/

[44] G. Banuppriya, R. Sribalan, V. Padmini, Synthesis and characterization of curcumin-sulfonamide hybrids: biological evaluation and molecular docking studies. J. Mol. Struct. (2018), 1155:90–100. DOI: 10.1016/j.molstruc.2017.10.097
[45] Suhailah Wasman Qader, A. Suvitha, Mehmet Ozdemir, Innocent Benjamin, Anu Sai Ram NSA, Martilda U. Akem, Ahuekwe Eze Frank, Emereze C. Eluwa, Investigating the physicochemical properties and pharmacokinetics of curcumin employing density functional theory and gastric protection, Chemical Physics Impact, Volume 5, (2022), 100130. https://doi.org/10.1016/j.chphi.2022.100130
[46] N. S. Venkataramanan, Suvitha, Y. Kawazoe, Intermolecular interaction in nucleobases and dimethyl sulfoxide/water molecules: A DFT, NBO, AIM and NCI analysis. Journal of Molecular Graphics and Modelling, 78, 48–60, (2017). DOI: 10.1016/j.jmgm.2017.09.022
[47] E.R. Johnson, S. Keinan, P. Mori-Sanchez, J. Contreras-Garcia, A.J. Cohen, W. Yang, Revealing noncovalent interactions, J. Am. Chem. Soc. 132 (2010) 6498–6506. https://doi.org/10.1021/ja100936w
[48] E. Nemati-Kande, R. Karimian, V. Goodarzi, E. Ghazizadeh, Feasibility of pristine, Al-doped and Ga-doped Boron Nitride nanotubes for detecting SF4 gas: A DFT, NBO and QTAIM investigation. Applied Surface Science. 510 (2020) 145490. https://doi.org/10.1016/j.apsusc.2020.145490
[49] A. D. Isravel, Jeyaraj, J. K, Thangasamy, W. J. John, DFT, NBO, HOMO-LUMO, NCI, stability, Fukui function and hole – Electron analyses of tolcapone, Computational and Theoretical Chemistry, 1202, 113296 (2021). doi:10.1016/j.comptc.2021.113296
[50] D.L. Lande, S.A. Bhadane, S.P. Gejji, Noncovalent interactions accompanying encapsulation of resorcinol within azacalix[4]pyridine macrocycle, J. Phys. Chem. 121 (2017) 1814–1824. DOI: 10.1021/acs.jpca.6b12912
[51] B. Silvi, A. Savin, Classification of chemical bonds based on topological analysis of electron localization functions, Nature 371 (1994) 683–686. DOI: 10.1038/371683a0
[52].M.Amalanathan, M.Sony Michael Mary, M.LathaBeatriced, S.MaryDelphine ,H.Marshan Robert, A.R.Twinkle, ZoranRatkovic, Y.Samson Molecular Simulation Vol. 48, 2022, 387–402
[53] M.Sony Michael Mary, R. RacilJeyaGeetha, M.Amalanathan, H.MarshanRobert, A.RonaldoAnuf Spectroscopy Letters 55, 2022
[54] M. Amalanathan, T. Brintha, S. Sijana, P.J. JeganBabu, M. Sony Michael Mary Chemical Physics Impact 7, 2023, 100393
[55]. Oleg Ursu, Anwar Rayan, Amiram Goldblum, Tudor I. Oprea, Understanding drug-likeness Wiley interdisciplinary reviews: Computational Molecular Science, 1(5):760 – 781. DOI:10.1002/wcms.52
[56]. G. Richard Bickerton, Gaia V. Paolini, Jérémy Besnard, Sorel Muresan, Andrew L. Hopkins, Quantifying the chemical beauty of drugs, Nat Chem. 4(2): 90–98, (2012). DOI: 10.1038/nchem.1243
[57] H. Tijjani, A. Olatunde, A.P. Adegunloye, A.A. Ishola, In silico insight into the interaction of 4-aminoquinolines with selected SARS-CoV-2 structural and nonstructural proteins, Coronavirus Drug

Discovery: Druggable Targets and In Silico Update: Volume 3: 313-333, (2022). ID: covidwho-2149151

[58] Arup Ghose, Knowledge-based chemoinformatic approaches to drug discovery, Drug Discovery Today, 11(23-24):1107-14, (2006). DOI: 10.1016/j.drudis.2006.10.012

[59]. C.A. Lipinski, Lead-and drug-like compounds: the rule-of-five revolution, Drug Discov. Technol. 1(4):337–341, (2004). doi: 10.1016/j.ddtec.2004.11.007

[60] Michael Berry, Burtram Fielding, Junaid Gamieldien, Practical Considerations in Virtual Screening and Molecular Docking, Emerging Trends in Computational Biology, Bioinformatics, and Systems Biology, 487–502, (2015). DOI: 10.1016/B978-0-12-802508-6.00027-2

[61] Kunal Roy, Supratik Kar, Rudra Narayan Das, Understanding the Basics of QSAR for Applications in Pharmaceutical Sciences and Risk Assessment, Academic Press, (2015). ISBN: 9780128016336